# Nitrogen-hydrogen-oxygen ternary phase diagram: New phases at high pressure from structural prediction

Jingming Shi,[1,2] Wenwen Cui,[1,2] Silvana Botti,[3,4,*] and Miguel A. L. Marques[4,5,†]

[1]*School of Physics and Electronic Engineering, Jiangsu Normal University, Xuzhou, China*

[2]*Institut Lumière Matière (UMR5306), Université Lyon 1-CNRS, Université de Lyon, F-69622 Villeurbanne Cedex, France*

[3]*Institut für Festkörpertheorie und -optik, Friedrich-Schiller-Universität Jena, Max-Wien-Platz 1, D-07743 Jena, Germany*

[4]*European Theoretical Spectroscopy Facility*

[5]*Institut für Physik, Martin-Luther-Universität Halle-Wittenberg, D-06099 Halle, Germany*

(Received 20 September 2017; revised manuscript received 30 November 2017; published 21 February 2018)

Using an *ab initio* evolutionary structural search, we predict two novel crystalline phases in the H-N-O ternary phase diagram at high pressure, namely, $NOH_4$ and $HNO_3$ (nitric acid). Our calculations show that the $C2/m$ phase of $NOH_4$ becomes stable at 71 GPa, while the $P2_1/m$ phase of $HNO_3$ stabilizes at 39 GPa. Both phases remain thermodynamically stable at least up to 150 GPa, the maximum pressure we considered. The $C2/m$ phase of $NOH_4$ contains two O-H layers and one dumbbell cluster layer, formed by two $NH_3$ molecules linked by a N-N covalent bond. The $P2_1/m$ phase of $HNO_3$ contains a surprising quasiclover layer formed of H-N-O covalent bonds. Further calculations show that both phases are semiconducting, with band gaps of 6.0 and 2.6 eV for $NOH_4$ and $NHO_3$, respectively. Our calculations also confirm that the compound $NOH_5$ ($NH_3H_2O$) becomes unstable at pressures above 122 GPa, decomposing into $NH_3$ and $H_2O$.

DOI: 10.1103/PhysRevMaterials.2.023604

## I. INTRODUCTION

Nitrogen, oxygen, and hydrogen are some of the simplest and better studied elements of the periodic table. Moreover, they are some of the most abundant elements in the solar system and form several textbook compounds, such as water, nitrogen oxides, ammonia, and nitric acid, that are fundamental not only to life, but also to modern industry [1–5]. The ternary phase diagram H-N-O is extremely well characterized as a function of composition and temperature at ambient pressure. There is also a large amount of studies, both experimental and theoretical, focused on the binary phase diagrams H-N, H-O, and N-O from room to very high pressures [6–8]. However, much less is still known about the ternary phase diagram under pressure.

Our aim is therefore to report in this article a systematic study of the ternary H-N-O phase diagram as a function of pressure. Our theoretical tool is global structural prediction. Structural prediction methods have proved for the past years to be extremely powerful to determine ground-state crystal structures under high pressure. They have already yielded a remarkable number of important results. For example, they were used to show that the xenon apparently missing from the Earth is in fact bound with iron at the interior of our planet [9], or that simple alkali metals become semiconducting and transparent under pressure [10]. More recently, structural prediction was able to find superconductivity with a record transition temperature in hydrogen sulfide [11,12], a prediction that was confirmed experimentally one year later [13].

It is easy to understand the importance and attractiveness of structural prediction in the field of high-pressure physics. In fact, under high pressure, materials can modify substantially the chemistry, leading to novel and unexpected bonding patterns, often making intuitions based on our ambient pressure knowledge fail spectacularly. Computer simulations offer a faster and cost-efficient solution to prescreen the phase diagram of materials, before performing targeted complicated and expensive high-pressure experiments.

Several global structural prediction algorithms have been developed over the past decade, such as genetic algorithms [14–16], particle-swarm methods [17,18], random search [19], and the minima hopping method [20,21]. These methods are now ready for use in a number of freely available codes. It is therefore not surprising that global structural prediction studies of bulk solids under pressure have mushroomed over the past years. A large majority of these works concentrates on single stoichiometries or binary phase diagrams. Studies of ternary phase diagrams are instead rarer, due to the significantly larger number of possible compositions, and the consequent increase of the required computational effort.

## II. ELEMENTARY AND BINARY PHASE DIAGRAMS

The phase diagrams of elementary and binary phases made of hydrogen, nitrogen, and oxygen have been extensively studied, both experimentally and theoretically, in a wide range of pressures and temperatures. In the following, we will summarize briefly the current knowledge, starting with the elemental phases.

Hydrogen, as the first and arguably the simplest element of the periodic table, has attracted much attention since Wigner and Huntington proposed in 1935 that solid hydrogen

*silvana.botti@uni-jena.de

†miguel.marques@physik.uni-halle.de

 ©2018 American Physical Society

might dissociate into an atomic metal at around 25 GPa [1]. Unfortunately, the extremely weak x-ray scattering of hydrogen hindered for a long time the experimental studies of the low-temperature and high-pressure structures. Phase I of hydrogen consists of a disordered hcp structure [22], while the low-temperature and high-pressure phases II and III were extensively studied both experimentally and theoretically [19,23–30]. More recently, experimental results suggest a phase transition to a metallic, atomic phase at around 447 GPa [31], but these results are still under intense debate.

Nitrogen has a remarkably rich phase diagram, with no less than 13 solid molecular phases [2,32–38], an amorphous state [33], and two nonmolecular phases [39,40]. At 300 K, nitrogen freezes at 3 GPa to $\beta$-$N_2$, and further compression results in the $\delta$, $\delta_{\rm loc}$, $\epsilon$, $\zeta$, and $\kappa$ phases at 5, 11, 16, 60, and 115 GPa, respectively [3,4,34,41–43]. Finally, at about 150 GPa, there is a transition to the amorphous $\eta$ phase, which exhibits substantial pressure hysteresis [33,44]. Recently, Frost and co-workers synthesized a new phase, called $\lambda$-$N_2$, through low-temperature compression, and observed it to have a remarkably wide stability range [45].

Oxygen also exhibits a rich polymorphism with seven unambiguously established crystalline phases. At ambient pressure and as a function of temperature, oxygen solidifies to the paramagnetic $\gamma$ phase, then to the magnetically disordered $\beta$ phase [5,46], and ultimately to the antiferromagnetic $\alpha$ phase [47]. At a pressure of 6 GPa, the $\alpha$ phase transforms into the antiferromagnetic $\delta$ phase [48–50]. As the pressure increases to about 8 GPa, the $\delta$ phase of oxygen is destroyed, leading to the $\varepsilon$-$O_8$ phase, consisting of $O_8$ clusters [51,52]. Above 96 GPa, $\varepsilon$-$O_8$ was observed to transform into a metallic $\zeta$ phase [53,54] (that intriguingly exhibits superconductivity with a transition temperature of 0.6 K [55]). Zhu and co-workers predicted another phase of oxygen at 1.92 TPa, which exhibits polymeric spiral chains of $O_4$ [56]. These studies explored the high-pressure phase diagrams of solid oxygen up to a maximum pressure of 2 TPa.

Beside the elementary phase diagrams, also the binary N-H, N-O, and O-H diagrams have been extensively studied. The low-temperature and pressure phase I ($P2_13$) of $NH_3$ undergoes a first-order phase transition into phase IV ($P2_12_12_1$) at around 3–4 GPa and then into phase V at about 14 GPa [6–8]. In 2008, Pickard *et al.* found that the phase V of ammonia also belongs to the space group $P2_12_12_1$. Furthermore, they predicted two new ionic phases under high pressure ($Pma2$ and $P2_1/m$) that retransform into a molecular phase ($Pnma$) at about 440 GPa [57].

As one of the most important binary compounds, $H_2O$ ice has a very rich phase diagram. Until now at least 15 solid phases have been identified experimentally [58,59], and another seven high-pressure phases have been predicted by theoretical studies [60–63]. Experimentally, all crystalline phases were found to consist of water molecules connected by hydrogen bonds, except for ice-X. This latter is an atomic crystal and it is stable above 70 GPa at low temperature.

Nitrogen oxides such as NO, $N_2O_5$, $NO_2$, and $N_2O$ have also been studied both experimentally and theoretically. NO is a metastable compound at low pressure, while a polymeric NO structure becomes stable at 198 GPa [64]. Molecular $N_2O_5$ phases are stable in a wide pressure range from 9 to 446 GPa, when they decompose into NO and O [64]. The cubic phase ($Im\bar{3}$) of $NO_2$ forgoes two phase transitions at 7 GPa (to a $P2_1/c$ crystal) and then at 64 GPa (to an another $P2_1/c$ phase), before decomposing at 91 GPa [64]. $N_2O$ follows a series of phase transitions from $Pa\bar{3}$ [65] $\rightarrow$ $Cmca$ [66] $\rightarrow$ $C2m$ [67] $\rightarrow$ $P2_1/m$ [68] at the pressures of 57, 177, and 194 GPa, respectively.

Finally, for what concerns the literature on ternary compounds, the phase ammonia monohydrate (AMH) I [69] of $NH_3H_2O$ is known to transform into AMH II [70] at about 2.8 GPa. AMH II turns into a $P4/nmm$ and then into a $Ima2$ phase at 3.3 and 42 GPa [71], respectively. On the other hand, a new high-pressure phase ($P2_1/c$) of pure nitric acid ($HNO_3$) has been characterized at 1.6 GPa at room temperature by high-pressure neutron powder and x-ray single-crystal diffraction techniques by Allan and co-workers in 2010 [72].

## III. METHODS

For our study we chose to perform structural prediction using a particle-swarm optimization algorithm, implemented in the CALYPSO code [17,18]. This method is unbiased by any known structural information, and has been successfully used for the prediction of various systems under high pressure [73–76]. The underlying *ab initio* structural relaxations and the electronic band-structure calculations were performed in the framework of density functional theory (DFT) using the VASP code [77]. The calculations were carried out in the generalized gradient approximation for the exchange-correlation potential, using the Perdew-Burke-Ernzerhof [78] (PBE) functional. The electronic wave functions were expanded in a plane-wave basis set with a cutoff energy of 600 eV. The electron-ion interaction was described by means of projector augmented-wave (PAW) [79] pseudopotentials with $1s^1$, $2s^22p^3$, and $2s^22p^4$ electrons in the valence for the H, N, and O atoms, respectively. Monkhorst-Pack $k$-point [80] meshes with a grid density of $0.03\ \text{Å}^{-1}$ were chosen to achieve a total energy convergence of better than 1 meV per atom. The phonon dispersion curves were computed by the direct supercell calculation method, as implemented in the PHONOPY program [81].

We define a compound thermodynamically stable if its distance to the convex hull of stability is zero. We recall that the convex hull is a hypersurface in the composition space, that connects compounds that have a formation enthalpy lower than all possible decomposition channels. The (positive) distance to the convex hull of a phase measures its instability. Beside the newly predicted structures, we considered elementary, binary, and ternary phases already studied in theoretical and/or experimental works available in literature. To obtain reliable enthalpy differences, we recalculated the enthalpies of all these structures using our calculation setup. These calculations allowed us to confirm the phase ordering presented in previous theoretical studies on elementary and binary phases.

Note that our calculations are performed at zero temperature and in a range of pressures from 0 to 150 GPa. The inclusion of temperature effects would require the calculation of the phonon modes of all involved compounds in the whole pressure range. The very high computational cost associated with these

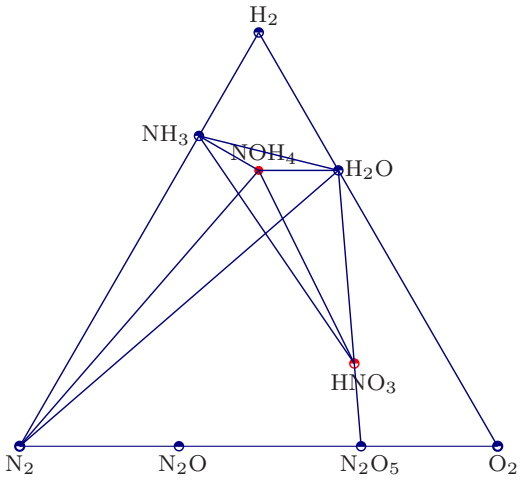


FIG. 1. Ternary phase diagram of the H-N-O system at 150 GPa. The novel phases are marked in red.

calculations explains why we focus in this work solely on the effects of pressure.

## IV. RESULTS

We investigated systematically the phase stability of stoichiometric $NOH_x$ ($x = 1, 2, 3, 4, 5$), $HON_x$ ($x = 1, 2, 3, 4, 5$), $HNO_x$ ($x = 1, 2, 3, 4, 5$), and $H_3NO_4$ compounds. The structural prediction runs were performed with unit-cell sizes of 2 and 4 formula units (f.u.) at pressures of 50, 100, and 150 GPa. To limit the computational burden, we decided to restrict our investigation to a limited set of stoichiometries that allowed one to keep the unit cells sufficiently small. We calculated the convex hull of thermodynamic stability with respect to the decomposition into all known phases of the H-N-O ternary system, including our theoretical predictions and the most stable phases reported experimentally and theoretically in the corresponding pressure range. The phases that we included explicitly to build the convex hull, as they belong to the lowest enthalpy decomposition channels, are $H_2$ ($P6_3/m$ and $C2/c$) [19], $N_2$ ($P4_12_12$ [39] and $I2_13$ [43]), $O_2$ ($C2/m$) [51,52], $H_2O$ (phase X [60] for the pressure above 70 GPa and phase VIII [58] below 70 GPa), $N_2O$ ($Pa\bar{3}$ [65] and $Cmca$ [66]), $N_2O_5$ ($P\bar{1}$ and $C2/c$) [64], and $NH_3$($P2_12_12_1$ for a pressure below 90 GPa and $Pma2$ above 90 GPa) [57].

In Fig. 1 we show the ternary phase diagrams of H-N-O at a pressure of 150 GPa (the largest pressure that we considered). Metastable compositions that appear above the convex hull are not plotted for clarity. There are several conclusions that we can immediately extract from Fig. 1. First, all compositions $HON_x$ ($x = 1, 2, 3, 4, 5$) are above the convex hull, which implies that they are not thermodynamically stable at 150 GPa. If we consider $HNO_x$ ($x = 1, 2, 3, 4, 5$), only $HNO_3$ (nitric acid) is on the convex hull, although in a novel structure different from the low-pressure phases. Finally, for $NOH_x$ ($x = 1, 2, 3, 4, 5$), the only stable composition is interestingly not $NOH_5$ (i.e., $NH_3H_2O$, a mixture of water and ammonia that is 0.098 eV/f.u. above the hull) but $NOH_4$. This is again an indication of the profound influence that high pressure has on the chemistry of even simple elements, leading to unexpected stoichiometries and bonding patterns.

The structures of the two novel phases that we have identified, $NOH_4$ and $HNO_3$, are shown in Fig. 2(a), and Figs. 3(a) and 3(b). We also plotted the charge density and electron localization functions of these two phase, as shown in Figs. 2(b) and 2(c) and Figs. 3(c) and 3(d), respectively. The structural parameters of the predicted stable structures for the H-N-O ternary system are summarized in Table I. In the following, we analyze systematically the two new phases.

We calculated the dependence of the formation enthalpy on the applied pressure, considering the possible decomposition of $NOH_5$ and $NOH_4$ into water, ammonia, and nitrogen, as shown in Fig. 4. We find that $NH_3H_2O$ is stable in a large range of pressures, in good agreement with previous works [71], but that it becomes thermodynamically unstable at around 122 GPa when it decomposes into $NH_3$ and $H_2O$. We find the opposite behavior for $NOH_4$, that becomes stable at around 71 GPa, as shown in Fig. 4.

The new phase of $NOH_4$ has $C2/m$ symmetry (space group No. 12), with 24 atoms in the unit cell as shown in Fig. 2(a). It is composed of O-H chains separated by a layer of $NH_3$ molecules. To understand the bonding character of this structure, we plot in Fig. 2(b) the charge density and in Fig. 2(c) the electron localization function (ELF). This latter quantity is

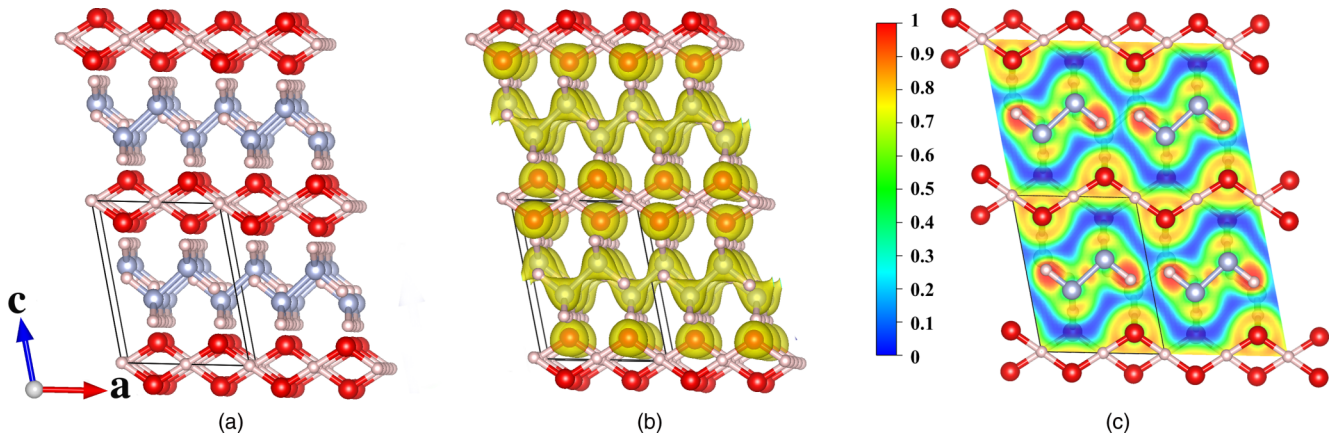


FIG. 2. (a) Crystal structure of $NOH_4$ with space group $C2/m$. The white, blue, and red atoms represent H, N, and O, respectively. (b) Charge density plot. (c) Electron localization function in the plane perpendicular to the (010) crystallographic direction.

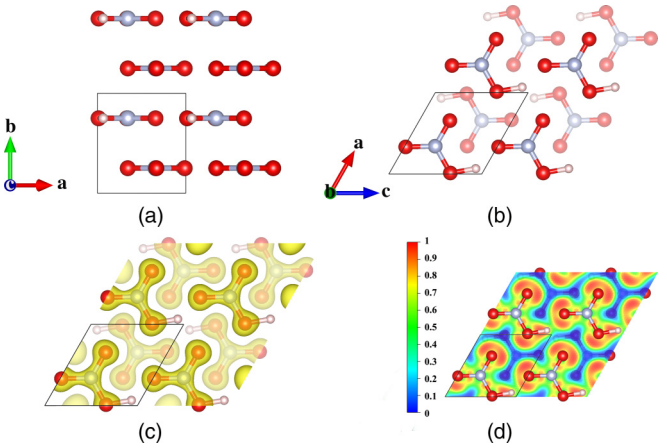


FIG. 3. (a), (b) The $P2_1/m$ phase of $HNO_3$. The red, light blue, and white atoms represent respectively O, N, and H. (c) Charge density plot of the $P2_1/m$ phase of $HNO_3$. (d) Slab cut along the (010) direction of the ELF. For clarity, we used here a $(2 \times 1 \times 2)$ supercell.

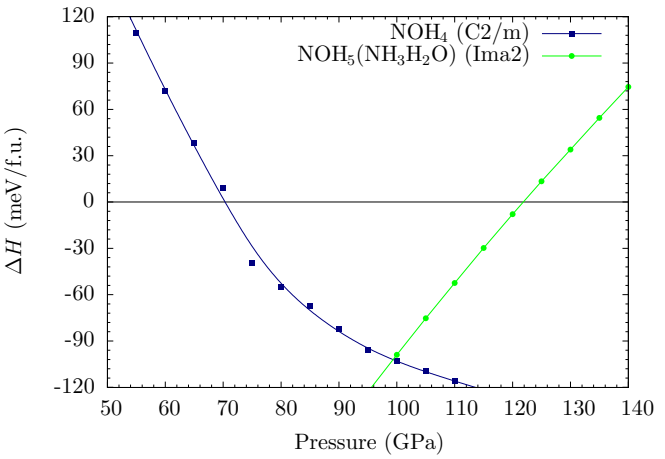


FIG. 4. Enthalpy per formula unit of the $Ima2$ phase of $NOH_5$ ($NH_3H_2O$) and of the $C2/m$ phase of $NOH_4$ as a function of pressure. The zero line corresponds to the decomposition into $NH_3$ and $H_2O$ (for $NOH_5$), or into $NH_3$, $H_2O$ and $N_2$ (for $NOH_4$).

a valuable tool developed in quantum chemistry to visualize bonds, lone pairs, etc. It assumes values in the range from zero to one, with one meaning perfect localization of electrons (such as in a bond). We find that the ELF has large values between two $NH_3$ molecules, indicating a covalent bond between the two N atoms. We thus conclude that the $NH_3$ layer is in fact built from $N_2H_6$ dumbbell clusters.

The H-O distance is 1.117 Å and the H-O-H angle is 112.87° at 150 GPa. In the chains, the electrons are mainly distributed in the center of the O-H bonds. The covalent character of these bonds can also be confirmed by the charge density plot in Fig. 2(b). On the other hand, the N-N distance is 1.355 Å at 150 GPa. We deduce that the N-N bond is a single bond, as confirmed by the shape of the ELF.

TABLE I. Predicted crystal structures of $NOH_4$ and $HNO_3$ at 150 GPa, and of $NOH_5$ at 100 GPa.

| Space group pressure | Lattice parameters | Atomic coordinates (fractional) |
|---|---|---|
| $C2/m$-$NOH_4$ | $a = 4.80513$ Å | H (8$j$) 0.73862 0.27769 0.18187 |
| 150 GPa | $b = 3.94998$ Å | H (2$a$) 0.00000 0.00000 0.00000 |
| | $c = 3.72274$ Å | H (2$b$) 0.00000 0.50000 0.00000 |
| | $\alpha = \gamma = 90°$ | H (4$i$) 0.47412 0.00000 0.83563 |
| | $\beta = 101.9°$ | O (4$i$) 0.86866 0.00000 0.21498 |
| | | N (4$i$) 0.60060 0.00000 0.65717 |
| $P2_1/m$-$HNO_3$ | $a = 3.76343$ Å | H (2$e$) 0.09859 0.25000 0.06669 |
| 150 GPa | $b = 3.71923$ Å | O (2$e$) 0.34502 0.25000 0.01337 |
| | $c = 3.79534$ Å | O (2$e$) 0.67110 0.25000 0.65678 |
| | $\alpha = \gamma = 90°$ | O (2$e$) −0.01431 0.25000 0.33338 |
| | $\beta = 119.7°$ | N (2$e$) 0.67195 0.25000 0.34246 |
| $Ima2$-$NOH_5$ | $a = 3.82308$ Å | H (8$h$) 0.00000 0.05335 0.26087 |
| ($NH_3H_2O$) | $b = 4.11076$ Å | H (8$i$) 0.27414 0.25000 0.02918 |
| 100 GPa | $c = 5.62304$ Å | H (4$d$) 0.25000 0.25000 0.75000 |
| | $\alpha = \beta = \gamma = 90°$ | O (4$e$) 0.00000 0.25000 0.86373 |
| | | N (4$e$) 0.00000 0.25000 0.37254 |

The $C2/m$ phase of $NOH_4$ at 150 GPa is dynamically stable as it does not exhibit any imaginary phonon frequencies, as shown in Fig. 5. The electronic band structure and projected density of states (DOS) are shown in Fig. 6. We observe that the $C2/m$ phase is an insulator with a large band gap of 6.0 eV at 150 GPa. Note that this value was calculated with the PBE functional, that systematically underestimate band gaps.

$HNO_3$ (nitric acid) at 150 GPa crystallizes in a novel phase of $P2_1/m$ symmetry and with an interesting structural configuration, containing two parallel layers forming a cloverlike pattern with a H atom tail. There are 10 atoms in the unit cell, as shown in Figs. 3(a) and 3(b). The "quasiclover" is formed by three nitrogen atoms, one oxygen atom, and one hydrogen atom. Every N atom in the middle of the quasiclover has three nearest O atoms, while one of the three O atoms is bonded with one H atom.

The charge density plot of the $P2_1/m$ phase of $HNO_3$ is shown in Fig. 3(c). We can clearly find that the electron cloud is almost entirely distributed around the region between the

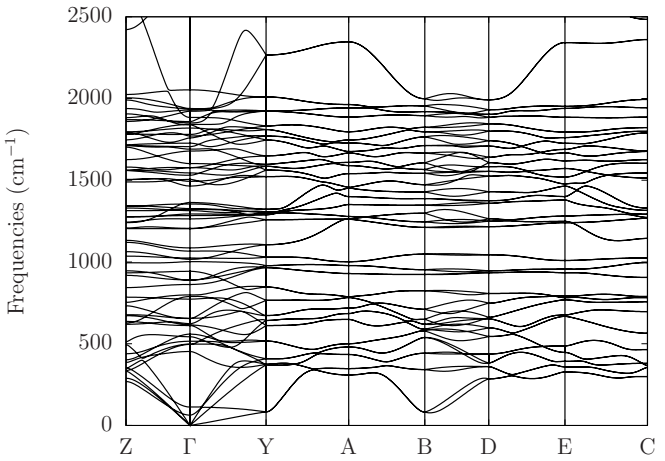


FIG. 5. Phonon dispersion of the $C2/m$ phase of $NOH_4$ at 150 GPa.

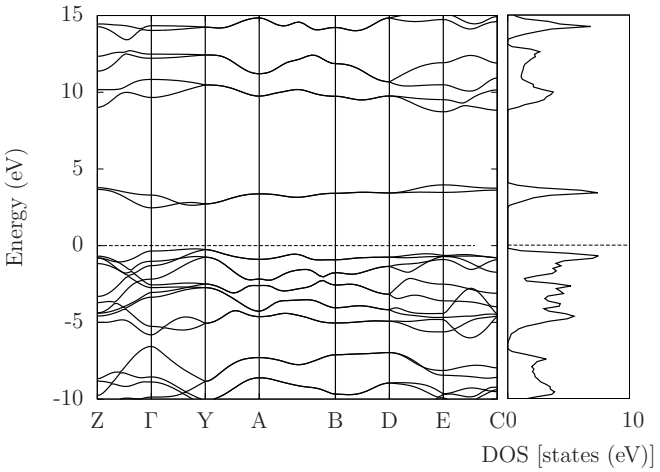


FIG. 6. Band structure and density of states of the $C2/m$ phase of $NOH_4$ at 150 GPa.

N and O atoms. Obviously, there are two different kinds of N-O covalent bonds, with bond lengths of 1.195 and 1.246 Å at 150 GPa. From the plot of the ELF [see Fig. 3(d)] one can distinguish the three N-O covalent bonds, together with the lone pairs around the oxygen atoms. The O-H bond distance is 1.042 Å at 150 GPa.

The relative enthalpy per formula unit of the new $P2_1/m$ phase of $HNO_3$, calculated with respect to the phase II ($P2_1/c$) [72], is shown in Fig. 7 as a function of pressure. Our results show that the new $P2_1/c$ phase is energetically favored in a large range of pressures from about 39 GPa to more than 150 GPa.

Finally, we calculated the phonon dispersion of this phase at 150 GPa, as depicted in Fig. 8, that proves that the $P2_1/m$ phase is mechanically stable. We also calculated the electronic band structure and density of states, as shown in Fig. 9. It reveals that the $P2_1/m$ phase of $HNO_3$ is a semiconductor with a PBE band gap of 2.6 eV.

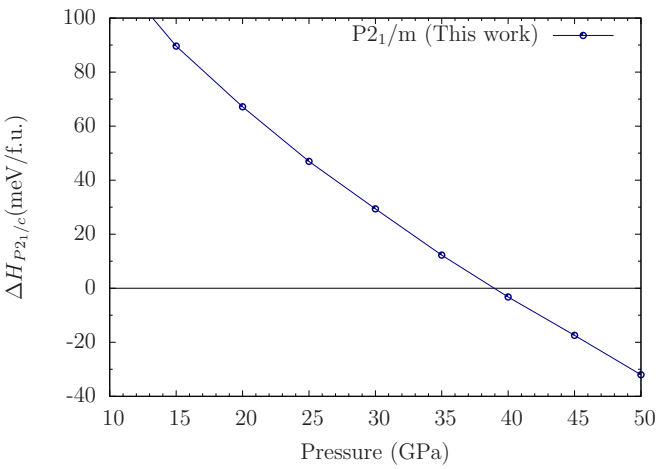


FIG. 7. Relative enthalpy per formula unit of the new phase $P2_1/m$ of $HNO_3$ with respect to phase II ($P2_1/c$) (see Ref. [72]) of nitric acid as a function of pressure.

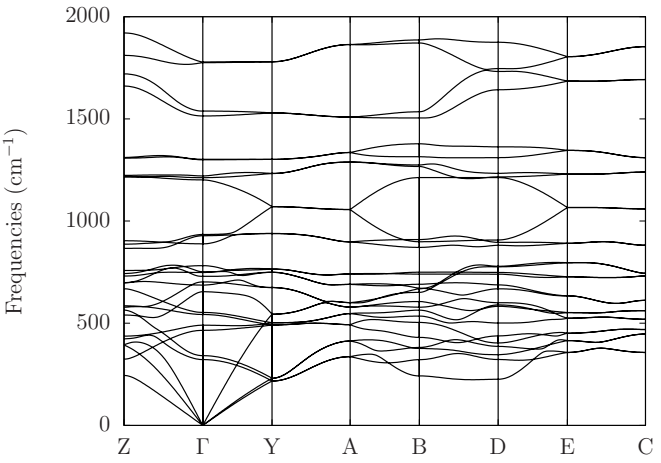


FIG. 8. Phonon dispersion of the $P2_1/m$ phase of $HNO_3$ at 150 GPa.

We observe that this work is an attempt to calculate from first principles the convex hull of stability of a ternary system with volatile elements. As in any other theoretical study of phase diagrams, we had to restrict ourselves to a number of different compositions and unit-cell sizes. As such, we cannot rule out the existence of other stable compounds with larger unit cells. If these undetected compounds have particularly low formation enthalpy, they may change significantly the shape of the convex hull of stability. However, and even in that case, we can still conclude that an experiment performed in the pressure range that we have suggested should detect new phases in the H-N-O phase diagram.

## V. CONCLUSION

In summary, we explored the ternary phase diagram of the H-N-O system at high pressure using a global structural prediction method combined with first-principles calculations. We found only two stable ternary phases at 150 GPa, namely, $NOH_4$ and $HNO_3$. The novel phase of $NOH_4$ possesses $C2/m$ symmetry while the new phase of $HNO_3$ has $P2_1/m$ symmetry.

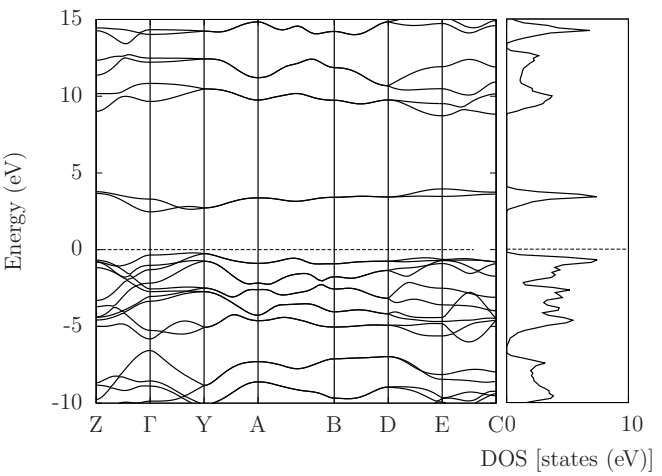


FIG. 9. Band structure and density of states of the $P2_1/m$ phase of $HNO_3$ at 150 GPa.

While the former composition becomes thermodynamically stable at 71 GPa, the $P2_1/m$ phase of $HNO_3$ is stabilized with respect to phase II at pressures higher than 39 GPa. Both are layered systems, with the $C2/m$ phase of $NOH_4$ containing HO chains separated by a $NH_3$-$NH_3$ dumbbell cluster, and the $P2_1/m$ phase of $HNO_3$ composed of quasiclovers, with a H tail. These structures are a consequence of the high pressure on the bonding behavior of even simple elements. Our results can be used as a guide for further experimental exploration of the ternary H-N-O phase diagram.

## ACKNOWLEDGMENTS

We thank A. San Miguel and S. Körbel for many fruitful discussions. J.S. and W.C. acknowledge financial support from the China Scholarship Council. M.A.L.M. acknowledges partial support from the DFG though Projects No. SFB-762 and No. MA-6786/1. Computational resources were provide by the Leibniz Supercomputing Centre through the SuperMuc Projects No. p1841a and No. pr62ja. The crystal structures were visualized with VESTA [82].

[1] E. Wigner and H. B. Huntington, J. Chem. Phys. **3**, 764 (1935).
[2] E. Gregoryanz, A. F. Goncharov, R. J. Hemley, H.-K. Mao, M. Somayazulu, and G. Shen, Phys. Rev. B **66**, 224108 (2002).
[3] W. E. Streib, T. H. Jordan, and W. N. Lipscomb, J. Chem. Phys. **37**, 2962 (1962).
[4] M. Hanfland, M. Lorenzen, C. Wassilew-Reul, and F. Zontone, Rev. High Press. Sci. Technol. **7**, 787 (1998).
[5] E. Hörl, Acta Crystallogr. **15**, 845 (1962).
[6] F. Datchi, S. Ninet, M. Gauthier, A. M. Saitta, B. Canny, and F. Decremps, Phys. Rev. B **73**, 174111 (2006).
[7] M. Gauthier, P. Pruzan, J. C. Chervin, and J. M. Besson, Phys. Rev. B **37**, 2102 (1988).
[8] M. Gauthier, P. Pruzan, J. C. Chervin, and A. Polian, Solid State Commun. **68**, 149 (1988).
[9] L. Zhu, H. Liu, C. J. Pickard, G. Zou, and Y. Ma, Nat. Chem. **6**, 644 (2014).
[10] Y. Ma, M. Eremets, A. R. Oganov, Y. Xie, I. Trojan, S. Medvedev, A. O. Lyakhov, M. Valle, and V. Prakapenka, Nature (London) **458**, 182 (2009).
[11] Y. Li, J. Hao, H. Liu, Y. Li, and Y. Ma, J. Chem. Phys. **140**, 174712 (2014).
[12] D. Duan, Y. Liu, F. Tian, D. Li, X. Huang, Z. Zhao, H. Yu, B. Liu, W. Tian, and T. Cui, Sci. Rep. **4**, 6968 (2014).
[13] A. Drozdov, M. Eremets, I. Troyan, V. Ksenofontov, and S. Shylin, Nature (London) **525**, 73 (2015).
[14] S. Woodley, P. Battle, J. Gale, and C. A. Catlow, Phys. Chem. Chem. Phys. **1**, 2535 (1999).
[15] N. L. Abraham and M. I. J. Probert, Phys. Rev. B **73**, 224104 (2006).
[16] A. R. Oganov and C. W. Glass, J. Chem. Phys. **124**, 244704 (2006).
[17] Y. Wang, J. Lv, L. Zhu, and Y. Ma, Phys. Rev. B **82**, 094116 (2010).
[18] Y. Wang, J. Lv, L. Zhu, and Y. Ma, Comput. Phys. Commun. **183**, 2063 (2012).
[19] C. J. Pickard and R. J. Needs, Nat. Phys. **3**, 473 (2007).
[20] S. Goedecker, J. Chem. Phys. **120**, 9911 (2004).
[21] M. Amsler and S. Goedecker, J. Chem. Phys. **133**, 224104 (2010).
[22] R. M. Hazen, H. K. Mao, L. W. Finger, and R. J. Hemley, Phys. Rev. B **36**, 3944 (1987).
[23] R. J. Hemley and H. K. Mao, Phys. Rev. Lett. **61**, 857 (1988).
[24] I. I. Mazin, R. J. Hemley, A. F. Goncharov, M. Hanfland, and H.-K. Mao, Phys. Rev. Lett. **78**, 1066 (1997).
[25] A. F. Goncharov, R. J. Hemley, and H.-k. Mao, J. Chem. Phys. **134**, 174501 (2011).
[26] S. T. John and D. D. Klug, Nature (London) **378**, 124 (1995).
[27] H. Kitamura, S. Tsuneyuki, T. Ogitsu, and T. Miyake, Nature (London) **404**, 259 (2000).
[28] P. Tolédano, H. Katzke, A. F. Goncharov, and R. J. Hemley, Phys. Rev. Lett. **103**, 105301 (2009).
[29] H. Liu and Y. Ma, Phys. Rev. Lett. **110**, 025903 (2013).
[30] H. Liu, L. Zhu, W. Cui, and Y. Ma, J. Chem. Phys. **137**, 074501 (2012).
[31] J. McMinis, R. C. Clay III, D. Lee, and M. A. Morales, Phys. Rev. Lett. **114**, 105305 (2015).
[32] R. Bini, L. Ulivi, J. Kreutz, and H. J. Jodl, J. Chem. Phys. **112**, 8522 (2000).
[33] E. Gregoryanz, A. F. Goncharov, R. J. Hemley, and H. K. Mao, Phys. Rev. B **64**, 052103 (2001).
[34] E. Gregoryanz, A. F. Goncharov, C. Sanloup, M. Somayazulu, H. K. Mao, and R. J. Hemley, J. Chem. Phys. **126**, 184505 (2007).
[35] M. J. Lipp, J. P. Klepeis, B. J. Baer, H. Cynn, W. J. Evans, V. Iota, and C.-S. Yoo, Phys. Rev. B **76**, 014113 (2007).
[36] M. I. Eremets, R. J. Hemley, H. K. Mao, and E. Gregoryanz, Nature (London) **411**, 170 (2001).
[37] Y. Ma, A. R. Oganov, Z. Li, Y. Xie, and J. Kotakoski, Phys. Rev. Lett. **102**, 065501 (2009).
[38] X. Wang, Y. Wang, M. Miao, X. Zhong, J. Lv, T. Cui, J. Li, L. Chen, C. J. Pickard, and Y. Ma, Phys. Rev. Lett. **109**, 175502 (2012).
[39] M. I. Eremets, A. G. Gavriliuk, I. A. Trojan, D. A. Dzivenko, and R. Boehler, Nat. Mater. **3**, 558 (2004).
[40] D. Tomasino, M. Kim, J. Smith, and C.-S. Yoo, Phys. Rev. Lett. **113**, 205502 (2014).
[41] M. Eremets, A. Gavriliuk, N. Serebryanaya, I. Trojan, D. Dzivenko, R. Boehler, H. K. Mao, and R. J. Hemley, J. Chem. Phys. **121**, 11296 (2004).
[42] E. Gregoryanz, C. Sanloup, R. Bini, J. Kreutz, H. J. Jodl, M. Somayazulu, H.-k. Mao, and R. J. Hemley, J. Chem. Phys. **124**, 116102 (2006).
[43] C. J. Pickard and R. J. Needs, Phys. Rev. Lett. **102**, 125702 (2009).
[44] A. F. Goncharov, E. Gregoryanz, H.-k. Mao, Z. Liu, and R. J. Hemley, Phys. Rev. Lett. **85**, 1262 (2000).
[45] M. Frost, R. T. Howie, P. Dalladay-Simpson, A. F. Goncharov, and E. Gregoryanz, Phys. Rev. B **93**, 024113 (2016).
[46] R. Le Sar and R. D. Etters, Phys. Rev. B **37**, 5364 (1988).
[47] R. J. Meier and R. B. Helmholdt, Phys. Rev. B **29**, 1387 (1984).
[48] D. Schiferl, D. T. Cromer, L. A. Schwalbe, and R. L. Mills, Acta Crystallogr., Sect. B **39**, 153 (1983).

[49] F. A. Gorelli, M. Santoro, L. Ulivi, and M. Hanfland, Phys. Rev. B **65**, 172106 (2002).
[50] I. N. Goncharenko, O. L. Makarova, and L. Ulivi, Phys. Rev. Lett. **93**, 055502 (2004).
[51] H. Fujihisa, Y. Akahama, H. Kawamura, Y. Ohishi, O. Shimomura, H. Yamawaki, M. Sakashita, Y. Gotoh, S. Takeya, and K. Honda, Phys. Rev. Lett. **97**, 085503 (2006).
[52] L. F. Lundegaard, G. Weck, M. I. McMahon, S. Desgreniers, and P. Loubeyre, Nature (London) **443**, 201 (2006).
[53] S. Desgreniers, Y. K. Vohra, and A. L. Ruoff, J. Phys. Chem. **94**, 1117 (1990).
[54] Y. Akahama, H. Kawamura, D. Häusermann, M. Hanfland, and O. Shimomura, Phys. Rev. Lett. **74**, 4690 (1995).
[55] K. Shimizu, K. Suhara, M. Ikumo, M. Eremets, and K. Amaya, Nature (London) **393**, 767 (1998).
[56] L. Zhu, Z. Wang, Y. Wang, G. Zou, H.-k. Mao, and Y. Ma, Proc. Natl. Acad. Sci. U.S.A. **109**, 751 (2012).
[57] C. J. Pickard and R. J. Needs, Nat. Mater. **7**, 775 (2008).
[58] V. F. Petrenko and R. W. Whitworth, *Physics of Ice* (Oxford University Press, Oxford, U.K., 1999).
[59] C. G. Salzmann, P. G. Radaelli, E. Mayer, and J. L. Finney, Phys. Rev. Lett. **103**, 105701 (2009).
[60] M. Benoit, M. Bernasconi, P. Focher, and M. Parrinello, Phys. Rev. Lett. **76**, 2934 (1996).
[61] B. Militzer and H. F. Wilson, Phys. Rev. Lett. **105**, 195701 (2010).
[62] Y. Wang, H. Liu, J. Lv, L. Zhu, H. Wang, and Y. Ma, Nat. Commun. **2**, 563 (2011).
[63] C. J. Pickard, M. Martinez-Canales, and R. J. Needs, Phys. Rev. Lett. **110**, 245701 (2013).
[64] D. Li, A. R. Oganov, X. Dong, X.-F. Zhou, Q. Zhu, G. Qian, and H. Dong, Sci. Rep. **5**, 16311 (2015).
[65] W. C. Hamilton and M. Petrie, J. Phys. Chem. **65**, 1453 (1961).
[66] R. Mills, B. Olinger, D. Cromer, and R. LeSar, J. Chem. Phys. **95**, 5392 (1991).
[67] C. Zhu, H. Bi, S. Zhang, S. Wei, and Q. Li, RSC Adv. **5**, 65745 (2015).
[68] Q. An, H. Xiao, W. A. Goddard III, and X. Meng, J. Phys. Chem. Lett. **5**, 485 (2014).
[69] I. Olovsson and D. H. Templeton, Acta Crystallogr. **12**, 827 (1959).
[70] A. D. Fortes, E. Suard, M.-H. Lemee-Cailleau, C. J. Pickard, and R. J. Needs, J. Am. Chem. Soc. **131**, 13508 (2009).
[71] A. Mafety, Étude ab initio des glaces d'ammoniac fluoré et hydraté sous conditions thermodynamiques extrêmes, Ph.D thesis, Université Pierre et Marie Curie, 2016.
[72] D. Allan, W. Marshall, D. Francis, I. Oswald, C. Pulham, and C. Spanswick, Dalton Trans. **39**, 3736 (2010).
[73] W. Cui, J. Shi, H. Liu, Y. Yao, H. Wang, T. Iitaka, and Y. Ma, Sci. Rep. **5**, 13039 (2015).
[74] J. Lv, Y. Wang, L. Zhu, and Y. Ma, Phys. Rev. Lett. **106**, 015503 (2011).
[75] F. Peng, M. Miao, H. Wang, Q. Li, and Y. Ma, J. Am. Chem. Soc. **134**, 18599 (2012).
[76] J. Shi, W. Cui, J. A. Flores-Livas, A. San-Miguel, S. Botti, and M. A. Marques, Phys. Chem. Chem. Phys. **18**, 8108 (2016).
[77] G. Kresse and J. Hafner, Phys. Rev. B **47**, 558 (1993).
[78] J. P. Perdew, K. Burke, and M. Ernzerhof, Phys. Rev. Lett. **77**, 3865 (1996).
[79] G. Kresse and D. Joubert, Phys. Rev. B **59**, 1758 (1999).
[80] H. J. Monkhorst and J. D. Pack, Phys. Rev. B **13**, 5188 (1976).
[81] A. Togo, F. Oba, and I. Tanaka, Phys. Rev. B **78**, 134106 (2008).
[82] K. Momma and F. Izumi, J. Appl. Crystallogr. **44**, 1272 (2011).